Published in Proceedings of the XVth International Congress of Theoretical and Applied Mechanics (Postprints), Toronto, Canada, August 17-23, 1980, edited by F.P.J. Rimrott and B. Tabarrok, North-Holland Publishing Company, 1980

SELF-SIMILAR SHAPES AND ASYMPTOTIC DILATATION-RATES FOR VOIDS IN VISCOUS SOLIDS

Bernard Budiansky and John W. Hutchinson

Division of Applied Sciences, Harvard University
Cambridge, Massachusetts 02138, USA

The growth-rate and shape are determined for an isolated void growing in a self-similar way in an infinite block of incompressible power-law, viscous material. The remote stress state is chosen to be axisymmetric, and the effects on void shape and growth-rate of various combinations of remote mean and deviatoric stress are studied. It is found that, with the superposition of a sufficiently high remote mean tensile stress, remote tensile stretching can produce oblate asymptotic voids which expand more slowly in the direction of stretching than in directions perpendicular to the stretching axis.

1. INTRODUCTION

This paper continues a study initiated in a previous paper [1] in which aspects of the growth or collapse of an initially spherical void in an infinite block of linearly or non-linearly viscous solid were studied. Under axisymmetric remote stressing conditions which cause the void to enlarge, the void approaches an asymptotic dilatation-rate and an asymptotic, or self-similar, shape which can be characterized as a pseudo-spheroid, a cylinder or a needle. In [1] the ranges of stress conditions which give rise to the three types of asymptotic shapes were determined, as were the dilatation-rates for the cylindrical and needle-like asymptotic void shapes. For the linearly viscous solid the asymptotic spheroidal shapes and their dilatation-rates were determined as well. They were not calculated for the nonlinearly viscous solid, however, and this is the objective of the present paper. We begin with a specification of the problem and a brief recapitulation of the relevant results from [1].

The material is an incompressible, isotropic viscous solid characterized in simple tension by

$$\dot{\varepsilon} = \dot{\varepsilon}_0(\sigma/\sigma_0)^n \tag{1.1}$$

where $\dot{\varepsilon}$ and σ are the tensile strain-rate and stress, $\dot{\varepsilon}_0$ and σ_0 are corresponding reference values, and the exponent n varies between unity (for a linearly viscous solid) and infinity (for a rigid-perfectly plastic solid). Under multi-axial stress states σ_{ij}, (1.1) is generalized to

$$\dot{\varepsilon}_{ij} = \frac{1}{2\eta}\sigma_e^{n-1}s_{ij} \tag{1.2}$$

where $\dot{\varepsilon}_{ij}$ is the strain-rate, s_{ij} is the stress deviator, $\sigma_e = (3s_{ij}s_{ij}/2)^{1/2}$ the effective stress, and η is a viscosity-like parameter defined by

$$\eta = \sigma_0^n/(3\dot{\varepsilon}_0) \tag{1.3}$$

As shown in Fig. 1, the void and the remote stresses are axisymmetric with respect to the x_3-axis. The remote stresses are specified by S and T where

$$\sigma_{11}^\infty = \sigma_{22}^\infty = T\ ,\ \sigma_{33}^\infty = S \tag{1.4}$$

It is also convenient to introduce the remote mean stress

$$\sigma_m = \frac{1}{3}\sigma_{ii}^\infty = \frac{1}{3}(S+2T) \tag{1.5}$$

and the quantity

$$\sigma = S - T \tag{1.6}$$

so that the remote effective stress is $\sigma_e^\infty = |\sigma|$. The remote strain-rate in the x_3-direction is

$$\dot{\varepsilon}_{33}^\infty \equiv \dot{\varepsilon}^\infty = \frac{1}{3\eta}|\sigma|^{n-1}\sigma \tag{1.7}$$

and the transverse strain-rates are

$$\dot{\varepsilon}_{11}^\infty = \dot{\varepsilon}_{22}^\infty = -\frac{1}{2}\dot{\varepsilon}^\infty \tag{1.8}$$

Evolution of the void under a fixed remote stress ratio S/T is considered. In this paper we will restrict consideration to cases in which both S and T are non-negative. Then, an initially spherical void grows in volume and, depending on S/T and n, becomes oblate or prolate and asymptotes to a shape which has either a finite or infinite aspect ratio a/b, where $2a$ is the length of the void along the axis of symmetry and b is its equatorial radius. With the current shape of the void specified by the polar-coordinate function $R(\theta)$ (see Fig. 1), the condition

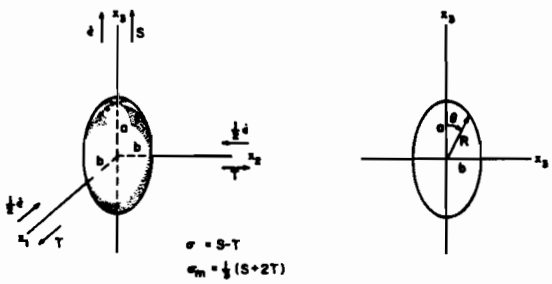

Fig. 1 Void geometry.

for an asymptotic, or self-similar, shape is

$$\dot{R}(\theta) = \tau R(\theta) \ , \ 0 \le \theta \le \pi \qquad (1.9)$$

A shape satisfying (1.9) is preserved under fixed S/T . The corresponding dilatation-rate of the asymptotic void is

$$\dot{V}/V = 3\tau \qquad (1.10)$$

where V is the volume of the void and $\dot{V}$ is its time-rate of change.

An initially spherical void in a linearly viscous solid (n = 1) deforms into an ellipsoid of revolution, i.e. a spheroid, and in [1] it was shown that the void evolves towards the following asymptotic shapes. For $0 \le T/S < 1/4$ with $S > 0$, the length 2a of the void grows without bound while the equatorial radius b diminishes to zero in such a way that the void volume is unbounded, except for $T = 0$ where the final to initial volume ratio is 1.26 . This asymptotic shape is accordingly designated a needle. For $1/4 < T/S \le 1/2$ with $S > 0$, both a end b are unbounded but a grows faster than b such that $a/b \to \infty$ as the void grows. For $T/S = 1/4$ b remains finite. In the range $1/4 \le T/S \le 1/2$, the asymptotic shapes are called cylinders. For both needles and cylinders the associated asymptotic dilatation-rate of the void is

$$\dot{V}/V = T/\eta \quad \text{for} \quad 0 \le T/S \le 1/2 \qquad (1.11)$$

When $\frac{1}{2} < T/S < 1$ with $S > 0$ and $n = 1$, the void evolves towards a prolate spheroid with an aspect ratio $\lambda = a/b > 1$ which satisfies

$$\frac{2S}{S+2T} = \lambda(\lambda^2-1)^{-3/2}\{\lambda(\lambda^2-1)^{1/2} - \cosh^{-1}\lambda\} \qquad (1.12)$$

For $1 < T/S < \infty$ with $S > 0$, the asymptotic void is an oblate spheroid whose aspect ratio λ satisfies

$$\frac{2S}{S+2T} = \lambda(1-\lambda^2)^{-3/2}\{\cos^{-1}\lambda - \lambda(1-\lambda^2)^{1/2}\} \qquad (1.13)$$

For $T/S = 1$ the void remains spherical. A plot of the asymptotic aspect ratios from (1.12) and (1.13) is given in Fig. 2. The dilatation-rate of these asymptotic voids was found in [1] to be identical to the corresponding initial dilatation-rate for a spherical void subject to the same S and T , i.e.

$$\frac{\dot{V}}{V} = \frac{3}{4\eta}\sigma_m = \frac{1}{4}\frac{(S+2T)}{\eta} \ , \ \frac{1}{2} < \frac{T}{S} < \infty \qquad (1.14)$$

As the void deforms from the starting spherical shape the dilatation-rate first drops slightly below (1.14) and then increases slowly back to the asymptote (1.14), as was illustrated in [1].

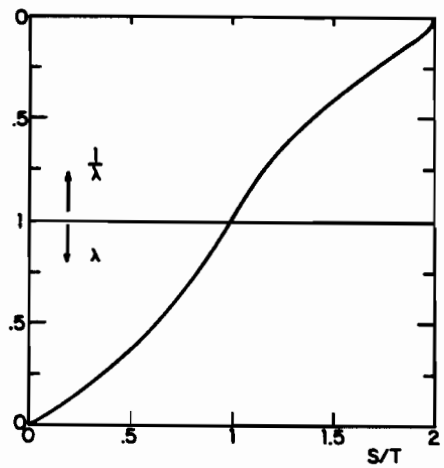

Fig. 2 Aspect ratio of asymptotic spheroidal void in linearly viscous solid.

Whether the material is linearly viscous (n = 1) or nonlinearly viscous (n > 1) the asymptotic shape will be a needle when the ratio of dilatation-rate to remote strain-rate $\dot{\epsilon}$ in (1.7) asymptotes to a value which is less than unity, i.e.

$$\frac{\dot{V}}{\dot{\epsilon}V} < 1 \quad \text{(for needles)} \qquad (1.15)$$

It was shown in [1] that when this inequality is satisfied the void elongates with decreasing equatorial radius, consistent with the definition of a needle-like asymptotic shape. For cylinders, the asymptotic limit of this ratio falls in the range

$$1 \le \frac{\dot{V}}{\dot{\epsilon}V} \le 3 \quad \text{(for cylinders)} \qquad (1.16)$$

while for

$$\frac{1}{\dot{\epsilon}}\frac{\dot{V}}{V} > 3 \qquad (1.17)$$

the asymptotic shapes are spheroids for $n = 1$ and pseudo-spheroids for $n > 1$.

For cylinders or needles, the relation between S/T and $\dot{V}/(\dot{\epsilon}V)$ is [1]

$$\frac{S}{T} = 1 + \left\{\frac{1}{\sqrt{3}}\int_0^{\dot{V}/(\sqrt{3}\dot{\epsilon}V)} [1+x^2]^{\frac{1-n}{2n}}\,dx\right\}^{-1} \qquad (1.18)$$

which gives

$$\frac{\dot{V}}{\dot{\epsilon}V} = \frac{3T}{S-T} \qquad (1.19)$$

for $n = 1$ and McClintock's [2] result

$$\frac{\dot{V}}{\dot{\epsilon}V} = \sqrt{3}\,\sinh\left[\frac{\sqrt{3}T}{S-T}\right] \qquad (1.20)$$

for the rigid-perfectly plastic material $(n = \infty)$, for which $|S-T| = \sigma_0$. The value of S/T corresponding to the transition between asymptotic shapes which are needles and cylinders is obtained from (1.18) with $\dot{V}/(\dot{\epsilon}V) = 1$ and is shown as a function of n in Fig. 3. Similarly, the transition from cylinders to pseudo-spheroids is given by (1.18) with $\dot{V}/(\dot{\epsilon}V) = 3$ and is also shown in Fig. 3.

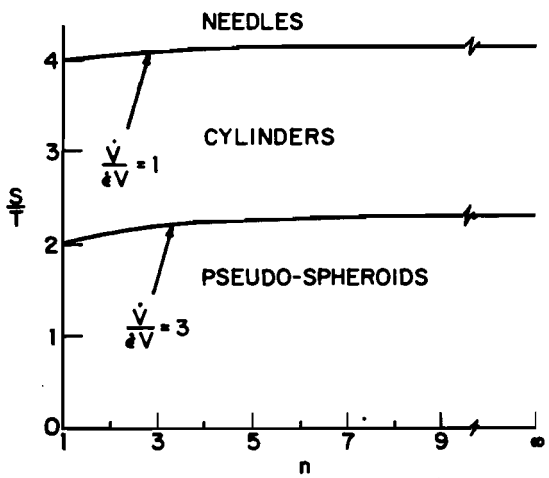

Fig. 3 Ranges of S/T for three types of asymptotic void shapes.

As mentioned above, the asymptotic pseudo-spheroids and their dilatation-rates were not determined in [1] for $n > 1$. We did, however, use a numerical method to determine the dilatation-rate of a spherical void in the non-linearly viscous solid, and these aphere results will be of use in the sequel. Under high triaxiality conditions in which both σ and σ_m are positive with $\sigma_m/\sigma > 1$, the normalized dilatation-rate is well approximated by the formula [1]

$$\frac{\dot{V}}{\dot{\epsilon}V} = \frac{3}{2}\left\{\frac{3}{2n}\frac{\sigma_m}{\sigma} + \frac{(n-1)(n+.432)}{n^2}\right\}^n \qquad (1.21)$$

This formula is exact for $n = 1$ and underestimates the large-n results by less than 10% for $\sigma_m/\sigma > 2$ and by less than 20% for $1 < \sigma_m/\sigma < 2$. For $n \to \infty$, (1.21) gives the result of Rice and Tracey [3] for a spherical void in a rigid-perfectly plastic solid under high triaxiality, i.e.

$$\frac{\dot{V}}{\dot{\epsilon}V} = .850\,\exp\left[\frac{3}{2}\frac{\sigma_m}{\sigma}\right] \qquad (1.22)$$

where $\sigma = \sigma_0$.

2. NUMERICAL PROCEDURE FOR DETERMINATION OF SELF-SIMILAR VOIDS

We first describe the procedure for calculating the velocity field and dilatation-rate of a void of specified shape and then go on to discuss the method used to seek the shape which satisfies the self-similarity condition (1.9).

A minimum principle for the velocity field suitable for the infinite region surrounding the traction-free void was given in [1]. Let $\underset{\sim}{\sigma}^\infty$ and $\dot{\underset{\sim}{\epsilon}}^\infty$ denote the remote stresses and strain-rates given in (1.4), (1.7) and (1.8) and let $\underset{\sim}{v}^\infty$ be the associated velocity field according to

$$\dot{\epsilon}^\infty_{ij} = \frac{1}{2}(v^\infty_{i,j} + v^\infty_{j,i}) \qquad (2.1)$$

An additional velocity field $\tilde{\underset{\sim}{v}}$ is introduced such that the total velocity is given by

$$\underset{\sim}{v} = \underset{\sim}{v}^\infty + \tilde{\underset{\sim}{v}} \qquad (2.2)$$

where $v_{i,i} = v^\infty_{i,i} = \tilde{v}_{i,i} = 0$. Then with

$$\dot{\epsilon}_{ij} = \frac{1}{2}(v_{i,j} + v_{j,i}) \quad \text{and} \quad \dot{\tilde{\epsilon}}_{ij} = \frac{1}{2}(\tilde{v}_{i,j} + \tilde{v}_{j,i}) \qquad (2.3)$$

the strain-rate is given by

$$\dot{\underset{\sim}{\epsilon}} = \dot{\underset{\sim}{\epsilon}}^\infty + \dot{\tilde{\underset{\sim}{\epsilon}}} \qquad (2.4)$$

If the additional velocity field decays faster than $r^{-1/2}$ for large $r = (x_i x_i)^{1/2}$, it minimizes

$$\Phi = \int_V [W(\dot{\underset{\sim}{\epsilon}}) - W(\dot{\underset{\sim}{\epsilon}}^\infty) - \sigma^\infty_{ij}\dot{\tilde{\epsilon}}_{ij}]\,dV - \int_S \sigma^\infty_{ij} n_j \tilde{v}_i\,dS \qquad (2.5)$$

where V is the region surrounding the void, S is the void surface, $\underset{\sim}{n}$ is the unit normal to S pointing into V , and

$$W(\dot{\underset{\sim}{\varepsilon}}) = \int_0^{\dot{\underset{\sim}{\varepsilon}}} \sigma_{ij} d\dot{\varepsilon}_{ij} = (3\eta)^{\frac{1}{n}} \left(\frac{n}{n+1}\right) \left(\frac{2}{3}\dot{\varepsilon}_{ij}\dot{\varepsilon}_{ij}\right)^{\frac{n+1}{2n}} \qquad (2.6)$$

In the limit $n \to \infty$ corresponding to rigid-perfect plasticity, the minimum principle based on (2.5) continues to hold but $\underset{\sim}{\sigma}^{\infty}$ must satisfy $s^{\infty}_{ij} s^{\infty}_{ij} = 2\sigma_0^2/3$ and $\dot{\varepsilon}^{\infty}_{ij}(\propto s^{\infty}_{ij})$ must be prescribed. In this limit the principle is the same as that used by Rice and Tracey [3] in their analysis of a spherical void.

With reference to Fig. 4, let $y = x_3$ be a coordinate aligned with the axis of symmetry of the void and let x be a radial coordinate coinciding with x_2 in the plane $x_1 = 0$. Let $z = x + iy$ be a complex variable defined in the physical trace plane shown, and let $\zeta = \xi + i\eta$ be a complex variable defined in terms of coordinates (ξ,η) in a mapping plane. Let

$$z = \omega(\zeta) = \frac{1}{\zeta} + c_1\zeta + c_2\zeta^3 + \ldots \qquad (2.7)$$

map the region exterior to the void in the plane of $x_1 = 0$ onto the interior of the unit circle in the ζ-plane. The coefficients c_i of the mapping function are real since the void trace is symmetric with respect to the y-axis and the search for a self-similar shape was restricted to voids which are symmetric with respect to the plane $x_3 = 0$.

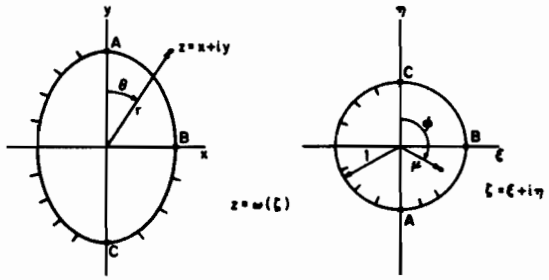

Fig. 4 Mapping geometry.

As shown in Fig. 4, let (r,θ) be planar-polar coordinates in the physical trace plane and (μ,ϕ) be the corresponding coordinates in the mapping plane, where both θ and ϕ are measured from the vertical in the clockwise sense. The additional velocity components can be derived from a stream function $\chi(r,\theta)$ according to

$$\tilde{v}_r = -r^{-2}(\sin\theta)^{-1}(\chi \sin\theta)_{,\theta}\ ,\ \tilde{v}_\theta = r^{-1}\chi_{,r} \qquad (2.8)$$

or

$$\tilde{v}_x = r^{-1}\chi_{,y} - yr^{-3}\chi\ ,\ \tilde{v}_y = -r^{-1}\chi_{,x} - y^2x^{-1}y^{-3}\chi \qquad (2.9)$$

The circumferential velocity component vanishes. Near the pole $\theta = 0$, it can be shown that χ must be of the form

$$\chi(r,\theta) = A\theta^{-1} + \theta f(r) + \theta^3 g(r) + \ldots \qquad (2.10)$$

Furthermore, the velocity field is symmetric with respect to $x_3 = 0$ and thus χ must be antisymmetric in θ with respect to $\theta = \pi/2$. A truncated complete representation for χ was employed. It was taken in the form

$$\chi = A\cot\theta + \sum_{k=1}^{N}\sum_{i=0}^{M} A_{ki}\frac{d}{d\phi}[P_{2k}(\cos\phi)]T_i(2\mu-1) \qquad (2.11)$$

where $P_j(\ )$ is the Legendre polynomial of degree j and $T_i(\ )$ is the Chebyshev polynomial of degree i. The amplitudes A and A_{ki} are free parameters which were chosen to minimize Φ. The lead term in (2.11) could equally well have been taken to be $A\cot\phi$; the choice made has numerical advantages, as will be discussed below.

The lead term in (2.11) gives a spherically symmetric velocity and strain-rate contribution with nonzero components

$$\tilde{v}_r = Ar^{-2}\ ,\ \dot{\tilde{\varepsilon}}_r = -\frac{1}{2}\dot{\tilde{\varepsilon}}_\theta = -\frac{1}{2}\dot{\tilde{\varepsilon}}_\alpha = -2Ar^{-3} \qquad (2.12)$$

where $\dot{\tilde{\varepsilon}}_\alpha$ is the circumferential component of the additional strain-rate. The contributions from the remaining terms in (2.11) to the velocities and strain-rates were computed using the change of variables from (x,y) to (μ,ϕ) specified by the mapping function (2.7). The expressions for the additional velocity and strain-rate components in the cylindrical coordinate system (x,α,y) involve χ, $\chi_{,x}$, $\chi_{,y}$, $\chi_{,xx}$, $\chi_{,xy}$ and $\chi_{,yy}$. By the change of variables,

$$\chi_{,x} = \chi_{,\mu}\frac{\partial\mu}{\partial x} + \chi_{,\phi}\frac{\partial\phi}{\partial x} \qquad (2.13)$$

$$\chi_{,xx} = \left(\chi_{,\mu\mu}\frac{\partial\mu}{\partial x} + \chi_{,\mu\phi}\frac{\partial\phi}{\partial x}\right)\frac{\partial\mu}{\partial x} + \chi_{,\mu}\frac{\partial^2\mu}{\partial x^2} + \left(\chi_{,\phi\mu}\frac{\partial\mu}{\partial x} + \chi_{,\phi\phi}\frac{\partial\phi}{\partial x}\right)\frac{\partial\phi}{\partial x} + \chi_{,\phi}\frac{\partial^2\phi}{\partial x^2} \qquad (2.14)$$

with similar expressions for the other partial derivatives of χ. Using the mapping function

(2.7), one can show that

$$\frac{\partial \mu}{\partial x} + i \frac{\partial \mu}{\partial y} = \mu \frac{\Omega}{|\Omega|^2} , \quad \frac{\partial \phi}{\partial y} - i \frac{\partial \phi}{\partial x} = - \frac{\Omega}{|\Omega|^2} \tag{2.15}$$

$$\frac{\partial^2 \mu}{\partial x^2} + i \frac{\partial^2 \mu}{\partial x \partial y} = \frac{\partial \mu}{\partial x} \frac{\Omega}{|\Omega|^2} + \mu \frac{\Omega'}{|\Omega|^2 \omega'} - \frac{2\mu\Omega}{|\Omega|^4} \mathrm{Re}\left[\frac{\bar{\Omega}\Omega'}{\omega'}\right] \tag{2.16}$$

$$\frac{\partial^2 \mu}{\partial x \partial y} + i \frac{\partial^2 \mu}{\partial y^2} = \frac{\partial \mu}{\partial y} \frac{\Omega}{|\Omega|^2} + i \frac{\mu\Omega'}{|\Omega|^2 \omega'} - \frac{2\mu\Omega}{|\Omega|^4} \mathrm{Re}\left[\frac{i\bar{\Omega}\Omega'}{\omega'}\right] \tag{2.17}$$

$$\frac{\partial^2 \phi}{\partial x \partial y} - i \frac{\partial^2 \phi}{\partial x^2} = - \frac{\Omega'}{|\Omega|^2 \omega'} + \frac{2\Omega}{|\Omega|^4} \mathrm{Re}\left[\frac{\bar{\Omega}\Omega'}{\omega'}\right] \tag{2.18}$$

and

$$\frac{\partial^2 \phi}{\partial y^2} - i \frac{\partial^2 \phi}{\partial x \partial y} = - \frac{i\Omega'}{|\Omega|^2 \omega'} + \frac{2\Omega}{|\Omega|^4} \mathrm{Re}\left[\frac{i\bar{\Omega}\Omega'}{\omega'}\right] \tag{2.19}$$

where $\Omega = \omega' \zeta$, $( )' = d( )/d\zeta$ and $\bar{( )}$ denotes the complex conjugate.

The partial derivatives of the terms in the double sum in (2.11) for χ with respect to μ and ϕ are easily determined. Thus, with the aid of the above equations, the additional velocities and strain-rates associated with any point ζ could be computed if values of the amplitudes (A, A_{ki}) were specified. The contribution from the spherically symmetric field with amplitude A was included by using (2.12) directly rather than through the change of variables. This avoided numerical difficulties associated with computing differences between large, nearly equal numbers near the pole $(\theta = 0)$, which are particularly severe for this term because of its $1/\theta$ variation for small θ . ϕ in (2.5) was evaluated using numerical integration. The second term in (2.5) is readily expressed as an integral with respect to ϕ (with $\mu = 1$), and this was evaluated using a ten point Gaussian quadrature formula for $0 \leq \phi \leq \pi/2$. The first integral in (2.5) is a double integral in μ and ϕ . At each of ten Gaussian integration stations of μ , the integration with respect to ϕ was carried out with a ten point Gaussian quadrature formula. These values were then used in the ten point formula for the integration with respect to μ . Evaluation of Φ for spherical voids for several cases in which the integrations can be carried out in closed form gave 5 or 6 significant figure accuracy [1].

For a given shape specified by $z = \omega(\zeta)$, minimization of Φ with respect to the amplitude factors was achieved by a numerically implemented Newton-Raphson method. With the $K = 1 + N(M+1)$ amplitudes denoted collectively by $\{A_j\}$, the minimum condition is

$$\partial \Phi / \partial A_j = 0 \quad , \quad j = 1,K \tag{2.20}$$

With $\{A_j\}$ as an estimate of the solution to (2.20). the improved estimate, $\{A_j + \Delta A_j\}$, in the next iteration is obtained from

$$\sum_{m=1}^{K} \Delta A_m \partial^2 \Phi / \partial A_m \partial A_j = -\partial \Phi / \partial A_j \tag{2.21}$$

where the partial derivatives are evaluated at $\{A_j\}$. All partial derivatives in (2.20) and (2.21) were evaluated numerically using finite difference formulas [1].

The search for a shape satisfying the self-similarity condition (1.9) was formulated as follows. A shape is specified by the mapping coefficients c_i in (2.7). Given the velocity field for any such shape, it can be shown that

$$\dot{R}(\theta) = [v_x \sin(\theta - \beta) + v_y \cos(\theta - \beta)]/\cos \beta \tag{2.22}$$

where β is the angle between normal to the trace of the void surface at θ and the radial vector, taken positive in the counterclockwise sense, and given by

$$\beta = \theta - \phi + \gamma - \pi \tag{2.23}$$

where $e^{i\gamma} = \omega'/|\omega'|$. Let

$$\tau = \int_0^{\pi} \dot{R}(\theta) d\theta \div \int_0^{\pi} R(\theta) d\theta \tag{2.24}$$

and, for $i \geq 1$, let

$$F_i(c_1, c_2, \ldots) = \int_0^{\pi} [\dot{R}(\theta) - \tau R(\theta)] P_{2i}(\cos \theta) d\theta \tag{2.25}$$

The self-similarity condition may be restated as

$$F_i(c_1, c_2, \ldots) = 0 \quad , \quad i = 1,\infty \tag{2.26}$$

An approximately self-similar shape is obtained by restricting the mapping function to J unknown coefficients c_i and by truncating (2.26) to the first J equations. Given an estimate $\{c_i\}$ to the solution to the truncated set of equations, an improved estimate, $\{c_i + \Delta c_i\}$, is obtained from

$$\sum_{j=1}^{J} \frac{\partial F_i(\underset{\sim}{c})}{\partial c_j} \Delta c_j = -F_i(\underset{\sim}{c}) \tag{2.27}$$

As in the minimization process, all partial derivatives in (2.27) were evaluated numerically. Repeated application of (2.27) led to a solution to the truncated equations (2.26), assuming a reasonable starting guess was made and given that S/T fell in the range in which a solution exists. Integrations in (2.24) and (2.25) were performed using ten point Gaussian quadrature

formulas with ϕ as the integration variable.

The calculations entailed by the procedures described above are lengthy and judicious choices for the set of amplitude factors and the number of mapping coefficients had to be made. The experience gained in the calculations for the spherical void in [1] were relevant to the choice of N and M in (2.11). All calculations reported below were carried out with $N = 2$ and $M = 3$ for a total of 7 free amplitudes. With this choice (2.11) contains the exact solution for the linear problem for the sphere and, by numerical experimentation with different N and M, was found to give the dilatation-rate to within about 1% for large n. Convergence of the Newton-Raphson iterations was extremely rapid for $n \leq 5$, while for $n = 10$ and ∞ convergence was somewhat slower.

Calculations of the self-similar shapes were performed using either one (c_1) or two (c_1 and c_2) free mapping coefficients in (2.7). The difference in the results for the dilatation-rate and the aspect ratio $\lambda = a/b$ for the calculation based on just c_1 and that based on c_1 and c_2 was small in all cases checked, except for $\lambda > 1$ when n is large. Of course, for the linear material ($n = 1$) the solution involves only c_1 since the asymptotic void shape is a spheroid with aspect ratio (1.12) or (1.13). For $n = 1$, the method described above gave the aspect ratio λ for a given S/T to within a few percent as long as the aspect ratio was not greater than about $2\frac{1}{2}$. For larger λ the accuracy began to deteriorate and more terms in the truncated representation for χ would have been necessary to improve the accuracy. Comparison of the computed dilatation-rate with the exact result (1.14) was even more favorable. For all the n-values, the dilatation-rate was less sensitive to the choice of N and M and the number of mapping coefficients than was the aspect ratio.

3. NUMERICAL RESULTS

Computed values of the normalized dilatation-rate, $\dot{V}/(\dot{\varepsilon}V)$, and aspect ratio, $\lambda = a/b$, of the asymptotic voids are presented in Table I. Also included in the table is the value of $\dot{V}/(\dot{\varepsilon}V)$ from the high-triaxiality formula (1.21) for a spherical void. For $n \leq 5$ the computed values of $\dot{V}/(\dot{\varepsilon}V)$ for the asymptotic void are never more than 12% greater than the values from (1.21) for the sphere. A comparison of the results for the asymptotic voids with the more accurate results for the sphere in [1] reveals an even closer correspondence between the dilatation-rete of the asymptotic void and the sphere when $n \leq 5$. Thus, the exact coincidence of these two dilatation-rates for the linear solid ($n = 1$) mentioned in the Introduction applies reasonably well to the moderately nonlinear materials as well. For the rigid-perfectly plastic material ($n = \infty$) the high-triaxiality formula for the sphere underestimates the dilatation-rate for the asymptotic void by as much as 40% when $S/T = 2$.

Table I

n	S/T	$\dot{V}/\dot{\varepsilon}V$	λ	$(\dot{V}/\dot{\varepsilon}V)^*$
2	1.15	52.1	1.01	51.5
2	1.25	22.7	1.10	22.3
2	1.30	17.3	1.17	16.9
2	1.35	13.8	1.25	13.5
2	1.40	11.5	1.34	11.2
2	1.50	8.50	1.56	8.34
2	1.60	6.72	1.91	6.67
3	1.15	118.3	.92	116.2
3	1.25	39.0	.93	37.7
3	1.35	20.5	.99	19.7
3	1.45	13.4	1.11	12.7
3	1.55	9.82	1.28	9.32
3	1.65	7.68	1.53	7.34
3	1.75	6.25	1.85	6.09
5	1.15	345.7	.88	346.1
5	1.25	74.4	.80	72.0
5	1.35	32.8	.79	30.5
5	1.55	13.4	.92	12.0
5	1.75	7.99	1.29	7.21
5	1.85	6.53	1.57	6.06
10	1.15	1591.	.87	1453.
10	1.25	165.	.75	154.
10	1.35	53.1	.64	49.1
10	1.45	28.5	.64	24.5
10	1.65	13.5	.75	10.9
10	1.85	8.40	1.11	6.92
10	1.95	6.93	1.34	5.90
∞	1.25	560.	.70	555.
∞	1.45	47.4	.47	39.1
∞	1.65	19.3	.54	14.0
∞	1.85	11.8	.76	8.16
∞	2.05	8.23	1.02	5.84
∞	2.25	6.21	1.38	4.64

*from Equation (1.21)

The asymptotic dilatation-rate is plotted as $(\dot{V}/\dot{\varepsilon}V)^{-1}$ as a function of S/T in Fig. 5. For $\dot{V}/(\dot{\varepsilon}V) > 3$ the asymptotic shapes are pseudo-spheroids, as already emphasized, and in this range the curves in Fig. 5 are plotted from the values in Table I, except for the curve for $n = 1$ which derives from (1.14). For $1 < \dot{V}/\dot{\varepsilon}V \leq 3$ the asymptotic void shape is a cylinder and in this range the curves in Fig. 5 are obtained from (1.18). The numerical results in Table I for the pseudo-spheroids are limited to values of $\dot{V}/\dot{\varepsilon}V$ which are greater than about 6. In Fig. 5 we have filled in the intermediate range $3 < \dot{V}/\dot{\varepsilon}V < 6$ by smoothly extrapolating the sections of the curves obtained from Table I so that they are continuous with the curves for the cylindrical voids. The estimate of the curves in Fig. 5

which were presented previously in [1] are quite good, especially for the moderately nonlinear materials.

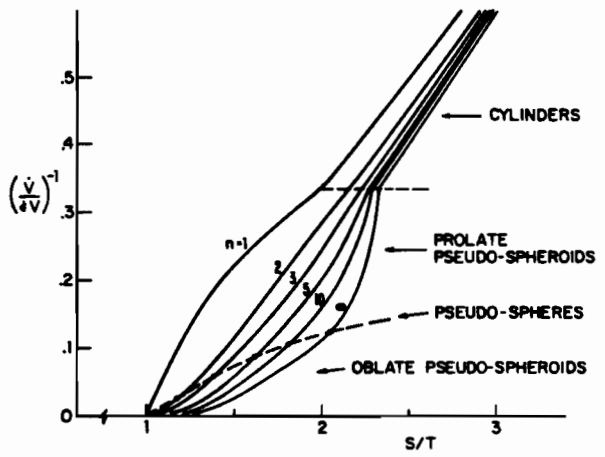

Fig. 5 Normalized dilatation-rates for the self-similar voids.

The aspect ratios of the asymptotic voids are displayed in Fig. 6. Based on the velocity fields for the sphere we anticipated in [1] that the asymptotic void in the nonlinear material would be oblate ($\lambda < 1$) under

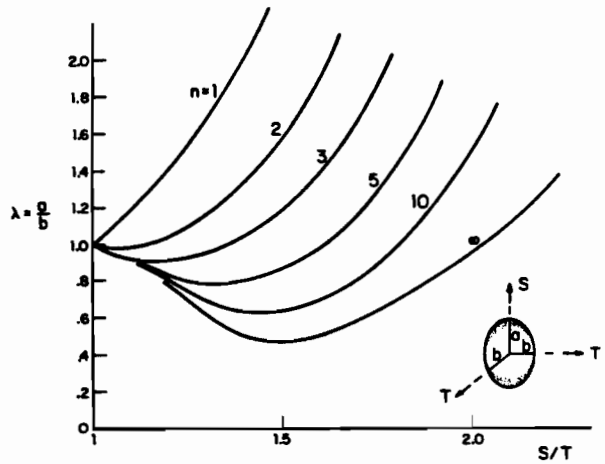

Fig. 6 Aspect ratios for the self-similar voids.

sufficiently high triaxiality. This speculation is indeed borne out. Oblateness is largest for the rigid-perfectly plastic material with a minimum value of λ of about .43 when $S/T = 1.5$ or, equivalently, when $\sigma_m/\sigma = 2.3$.

In this connection, it it interesting to note that the triaxiality level in the plastic zone at the tip of a plane strain crack is $\sigma_m/\sigma \approx 2$.

ACKNOWLEDGEMENT

This work was supported in part by the National Science Foundation under Grants DMR-77-24295 and ENG-78-10756, and by the Division of Applied Sciences, Harvard University.

REFERENCES

[1] Budiansky, B., Hutchinson, J. W. and Slutsky, S., Void Growth and Collapse in Viscous Solids, Harvard University Report, Division of Applied Sciences, MECH-15, February 1980, to be published in Mechanics of Solids, The Rodney Hill 60th Anniversary Volume, ed. by H. G. Hopkins and M. J. Sewell, Pergamon Press, 1981.

[2] McClintock, F. A., A criterion for ductile fracture by growth of holes, Trans. ASME, Series E, J. Appl. Mech. 35, 1968, 363-371.

[3] Rice, J. R. and Tracey, D. M., On the ductile enlargement of voids in triaxial stress fields, J. Mech. Phys. Solids 17, 1969, 201-217.